JOURNAL OF GEOPHYSICAL RESEARCH, VOL. 112, A12222, doi:10.1029/2007JA012254, 2007

Saturnian magnetospheric dynamics: Elucidation of a camshaft model

D. J. Southwood[1,2,3] and M. G. Kivelson[3,4]

Received 4 January 2007; revised 11 June 2007; accepted 17 August 2007; published 29 December 2007.

[1] Periodic modulation of magnetospheric phenomena at Earth and Jupiter results principally from the tilt of the dipole axis relative to the rotation axis. Saturn's nearly aligned dipole moment is tilted by less than 0.5° from the spin axis, yet the power of radio-frequency emissions, the orientation of the magnetic field, and many properties of the magnetospheric plasma vary periodically at the approximate rate of Saturn's rotation. Here we examine properties of the periodic magnetic signal detected in the magnetospheric regions inside ~12–15 R_S. We show that it is associated with a rotating nonaxisymmetric system of field-aligned currents flowing on magnetic shells bounding the region where the signals are seen. Magnetohydrodynamic ideas suggest that these currents would drive rotating plasma flow patterns in the northern and southern ionospheres, with the flows oppositely directed in the two hemispheres. On magnetic shells beyond the sheets of field-aligned current, the magnetic perturbations generate an effective rotating equatorial dipole moment that when added to the planetary dipole moment, produces a dipole moment tilted relative to the spin axis at an angle of order 12–15°. The overt source of the north–south asymmetric ionospheric circulation could link to different ionospheric conductances that result from nonuniform solar illumination. Other possible sources are discussed but, although we can elucidate much, the origin of the cam signal (as well as other phenomena such as the Saturn kilometric radio emission with close to the same period) remains enigmatic.

Citation: Southwood, D. J., and M. G. Kivelson (2007), Saturnian magnetospheric dynamics: Elucidation of a camshaft model, *J. Geophys. Res.*, *112*, A12222, doi:10.1029/2007JA012254.

1. Introduction

[2] Pioneer 11 and Voyager 1 and 2 measurements revealed that Saturn's magnetic field is very close to axially symmetric [*Smith et al.*, 1980a, 1980b; *Acuna and Ness*, 1980; *Acuna et al.*, 1981; *Ness et al.*, 1981; *Connerney et al.*, 1982]. This result has been confirmed through analysis of magnetometer data from the early orbits of Cassini [*Dougherty et al.*, 2005; *Giampieri et al.*, 2006], which constrain the dipole tilt to less than 0.5°. One would therefore not expect the field and plasma of the magnetosphere to vary at the period of planetary rotation. However, Saturn's radio emission in the kilometric wavelength band (referred to as SKR or Saturn kilometric radiation) was found to vary in intensity with a period of 10 h 39 min 24 s or 639.4 min [*Desch and Kaiser*, 1981] at the time of the Voyager flybys, a variation used to establish the official IAU rotation period. The cause of the intensity modulation has been hard to establish, with explanations usually invoking high-order magnetic anomalies. The challenge to understand the periodic variations became even greater after continued monitoring of SKR by the Ulysses spacecraft indicated that the period is not constant [*Lecacheux et al.*, 1997; *Galopeau and Lecacheux*, 2000] and led to suggestions that the solar wind can modify the period [e.g., *Cecconi and Zarka*, 2005]. The most recent evidence from Cassini (which arrived at Saturn in July 2004) suggests that the SKR period has varied during the first 2 years of this mission and is longer than the official IAU period [*Gurnett et al.*, 2005; *Kurth et al.*, 2007].

[3] It is not only the radio emissions that vary with a period close to that of planetary rotation. In 2000/2003, prior to the arrival in the Saturn system of the Cassini spacecraft, *Espinosa and Dougherty* [2000] and *Espinosa et al.* [2003a, 2003b] reanalyzed the magnetic field data obtained on the three pre-Cassini era flybys of Saturn (by Pioneer 11 and Voyager 1 and 2 spacecraft; see Figure 1) and demonstrated that the azimuthal component of the field was modulated at a period consistent with the rotation period inferred from radio measurements. As we shall describe in greater detail below, the periodic modulation of the magnetospheric magnetic field is even more evident in the Cassini data than in the data of the preceding spacecraft flybys. Espinosa and coworkers showed from polarization analysis that the signal cannot be accounted for by a small, previously undetected, residual tilt between planetary rotation and magnetic dipole axes. Detecting some evidence of

[1]European Space Agency Headquarters, Paris, France.
[2]Physics Department, Imperial College, London, UK.
[3]Institute of Geophysics and Planetary Physics, University of California, Los Angeles, California, USA.
[4]Department of Earth and Space Sciences, University of California, Los Angeles, California, USA.

0148-0227/07/2007JA012254$09.00

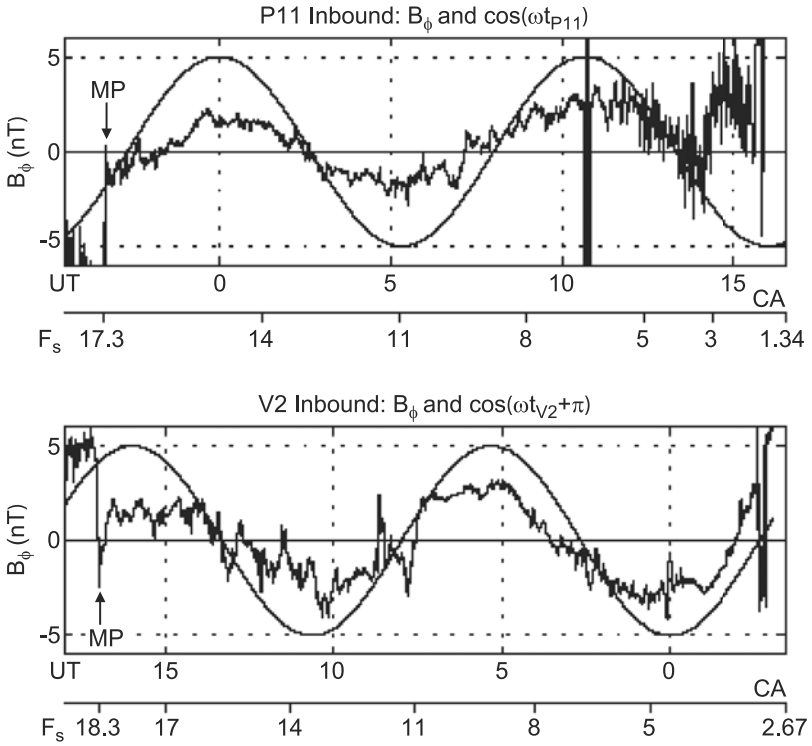

Figure 1. *Espinosa et al.* [2003a] examples of periodic variations of the azimuthal field component measured on the Pioneer 11 and Voyager 2 flybys of Saturn.

radially varying phase delays in signals, *Espinosa et al.* [2003a, 2003b] put forward a model suggesting that some asymmetry of planetary properties imposes a compressional signal that radiates outward through the plasma. They referred to their proposal as a camshaft model, recognizing that a camshaft acts to convert rotational motion into linear motion. As the planet rotates, alternating compressions and rarefactions propagate outward through the magnetosphere as compressional waves. *Cowley et al.* [2006] have confirmed the presence of the radial phase propagation indicated by *Espinosa et al.* [2003a, 2003b].

[4] The magnetometer data [*Dougherty et al.*, 2004] acquired during the first 2 1/2 years of Cassini's tour of Saturn are almost always modulated at a frequency comparable with the expected rotation rate of the planet over a large range of local times in the magnetosphere. Analyzing the magnetometer signal, *Giampieri et al.* [2006] estimated the period as 647.1 min ± 40 s. The estimate was based on magnetometer data acquired within a radial distance of less than 10 R_S (where R_S is Saturn's planetary radius = 60,268 km) from the first 14 months of orbital operations at Saturn. At that time, the uncertainty in period matched the variation that was predicted for the radio signal in the same interval. Since that time, it has become clear that the magnetic period varies slowly in time in a manner similar to the radio signals [*Gurnett et al.*, 2007].

[5] Particles reveal modulation at approximately the same period as the radio and magnetic field. Periodic intensifications on the night side of the magnetosphere are observed by Cassini's Magnetospheric Imaging Mass Spectrometer (MIMI) [*Paranicas et al.*, 2005; *Mitchell et al.*, 2006]. The region of intensification appears to rotate around the planet. The absence of dispersion of the flux bursts implies that they are regenerated in each rotation period.

[6] Given the clear evidence of periodic modulation of the magnetic field and other magnetospheric properties, it is the objective of this paper to analyze the symmetry, polarization, and phase relations between the transverse magnetic field components from data acquired near Cassini periapses, the camshaft signal, in order to elucidate further its origins.

[7] Despite the apparent link to the radio period, itself initially thought to be the rotation period of the planet, the cam signal is not associated with the internal field of the planet but has the properties of a field generated external to the planet [*Espinosa et al.*, 2003a]. We show further that the signal is confined to regions where the magnetospheric magnetic field is quasi-dipolar, that the signal is remarkably uniform in the radial range between 2.7 and 12–15 R_S and within the planetary latitude range $|\lambda| < 25°$ surveyed in the first two years of Cassini's tour around Saturn.

[8] We shall argue that the latitudinal symmetry of the camshaft field means that there is an interhemispheric exchange of momentum, which means any field-aligned current systems are unlike systems in other magnetospheres. The currents in question would flow on the magnetic shells with equatorial distances between 11–12 and 15 R_S. The cam field causes the total field to rock up and down through an angle that increases with radial distance. At any given distance, the rocking mimics the rocking that would be produced by the tilt (with respect to the rotation axis) of a centered dipole. Beyond the outer current-carrying shells the apparent tilt ceases to vary with distance. In this outer

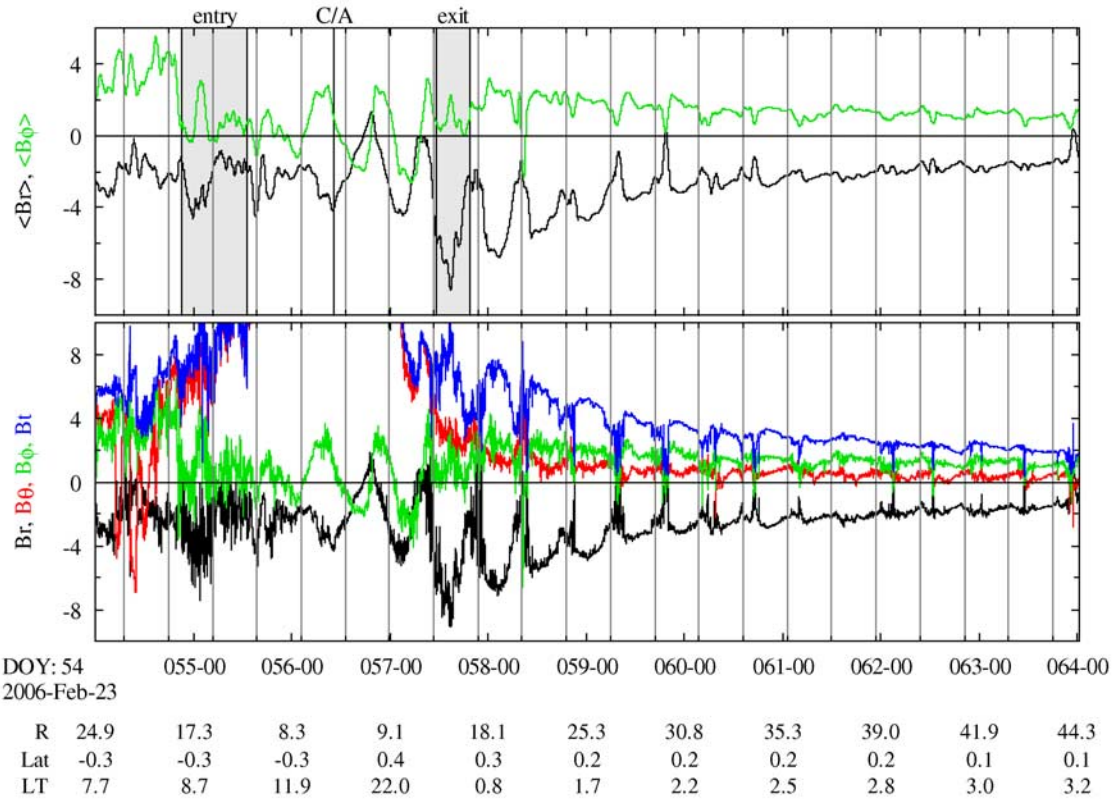

Figure 2a. Magnetometer data from a pass in February–March 2006 (periapsis 25 February) versus UT, showing (bottom) components of the field and the total field (color-coded) and (top) smooth fits (effectively a low pass filter) to the radial (black) and azimuthal (green) components. Radial distance in R_S, planetary latitude, and local time are indicated along the bottom. The field magnitude and the θ component go off scale near closest approach. Grid marks are spaced at 10 h 48.4 min which is the SKR periodicity predicted by long-term modeling of the signal *Kurth et al.* [2007]. In the inner portion of the pass between closest approach (C/A) and R $\sim$15 R_S, the peak in B_r leads the peak in B_ϕ. Beyond about 15 R_S on the nightside, the variations in B_r and B_ϕ are roughly in antiphase.

region, the field would be indistinguishable from that arising from a substantially tilted (12°–18°) centered dipole internal to the planet. It should be emphasized that the apparent tilt is dominated by the perturbations imposed by the external currents; how it could be linked to any true internal dipole remains to be shown.

2. Overview of Data

[9] In this section, we characterize the periodic variations of the structure of the Kronian magnetosphere as revealed by Cassini's FGM magnetometer [*Southwood et al.*, 1992; *Dougherty et al.*, 2004]. Data from two orbits in 2006 are shown in Figures 2a and 2b. For both spacecraft position and the field we use a polar coordinate system where the planetary spin axis is in the polar direction and the origin is at the center of the planet. The magnetic field data are plotted using a color-coded polar coordinate system [B_r (black), B_θ (red), B_ϕ (green)]. LT is local time in hours. R, in units of R_S, is the radial distance from the center of the planet and latitude is the angle (in degrees) between the radial vector and planetary equator. The regular vertical lines in all plots indicate the expected period of the Saturn kilometric radiation. The SKR period varies with time [*Lecacheux et al.*, 1997; *Galopeau and Lecacheux*, 2000]; markers are separated by the period computed from the formula given by *Kurth et al.* [2007]. For the February (June–July) pass the period is 648.4 min (648.6 min).

[10] Figures 2a and 2b illustrate a number of features that are found on most Cassini passes through the magnetosphere. We divide the magnetosphere into an inner region or core where the background field is predominantly dipolar (primarily in the B_θ direction) and the outer, distended region, where the field is primarily radially toward or away from the planet, the direction reversing across a near-equatorial current sheet. This magnetic field configuration is often referred to as "tail-like." In the outer magnetosphere of Saturn at dawn the field configuration is not confined to the nightside; the dawn outer magnetospheric field is usually tail-like and the configuration is often present even on the morningside. In Figure 2a, the distended field region is present only for some 8 h after the last magnetopause crossing and before the possible start of the transition region. On some other dayside passes around dawn, the outer edge of the cam is found much closer to the magnetopause. Normally, however, there is a rather extended region outside the cam but within the magnetopause.

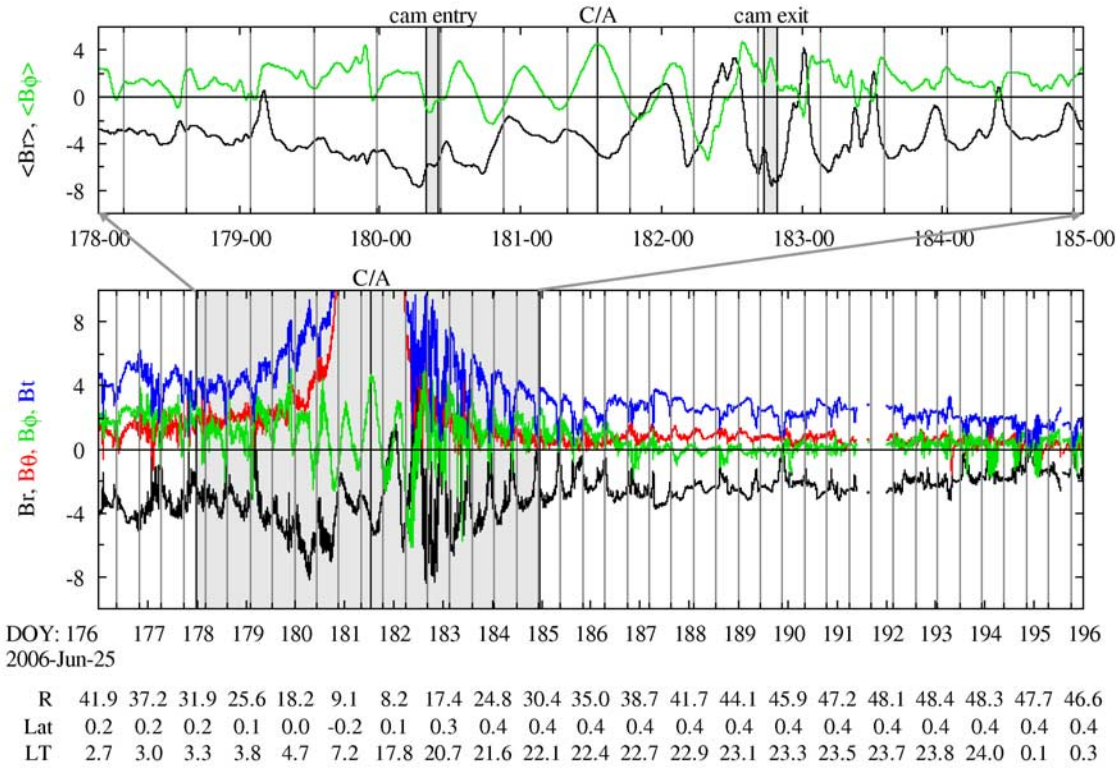

Figure 2b. Magnetometer data from a pass in June–July 2006 (periapsis on 30 June (C/A)) versus UT, showing (bottom) position (radial distance in R_S), planetary latitude, and local time. Almost a complete orbit is shown. Also shown is (top) an expanded plot of the radial (black) and azimuthal (green) components for 7 d around closest approach as indicated. The cam region is identified where the radial peak leads azimuthal fields roughly in quadrature. Entry and exit are marked. Coordinates for the field are once again polar coordinates based on the planetary axis and equatorial plane. Grid marks are spaced at 10 h 48.6 min which is the SKR periodicity predicted by long-term modeling of the signal [*Kurth et al.*, 2007].

[11] In the distended field region, periodicity is evident inbound in the morning hours, outbound near dawn and earlier in the night in the dipole-dominated region that we refer to as the core magnetosphere. The periodicity is not sinusoidal but certainly the period is comparable to the SKR period as the markers show. Indeed, as was noted by *Espinosa et al.* [2003] and confirmed by *Cowley et al.* [2006], there is a slight difference detectable in the periodicity outbound from inbound indicating a Doppler shift associated with an outward propagating signal.

[12] Over much of the distended magnetosphere, the mean B_ϕ remains positive, which, with B_r negative as it is predominantly in the plots, means that the equatorial portions of a magnetic flux tube lag the higher latitude portions and the field bends back relative to meridian planes. Such field configurations are consistent with flow that lags corotation, a situation that develops when there is net outward radial mass transport. The amplitudes of the B_r and B_ϕ oscillations change little with radial distance. They are comparable in magnitude and the two components are in antiphase (i.e., 180° phase difference), much as they are in the outer regions of Jupiter's near-equatorial magnetosphere [*Khurana*, 1997]. Not only do the amplitudes vary little with radial distance but also, near the equator, the periodic signal varies little with local time over the range that has been encountered thus far in the mission. (Cassini data coverage does not yet include the dusk sector at any great distance from the planet.)

3. Core (Cam) Region

[13] The periodicity persists during passage through closest approach where B_θ is the dominant background field. We call this the core region. This is where the cam field appears to be sited and it is the behavior of the field in this region that is the major topic of this paper. The signal is distinctly different from that in the distended magnetosphere. Most evident is the different phase relation between B_r and B_ϕ; B_ϕ and B_r perturbations are nearly in quadrature (i.e., 90° out of phase) with B_r leading. However the periodicity is distinctly different from the SKR period because there is a large Doppler shift associated with phase approaching periapsis where the angular velocity of the spacecraft becomes a substantial fraction of that of planetary rotation. The quadrature phase relation means that the field vector appears to rotate around the spin axis of the planet in the sense of planetary rotation as shown in the hodogram in Figure 3. The transition from one type of phase relation to

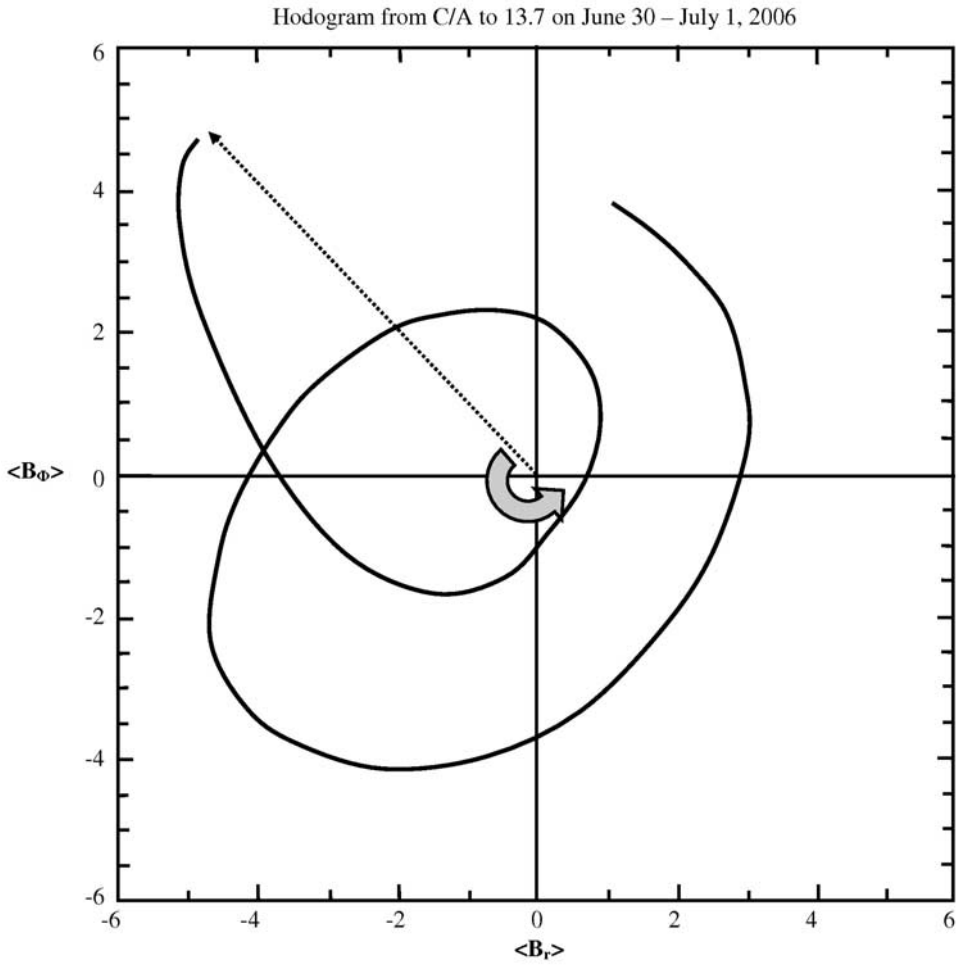

Figure 3. Hodogram of smoothed (with 6 h running average) B_r and B_ϕ components from C/A to 13.7 R_S on pass of June–July 2006 shown in Figure 2. The thick arrow indicates the sense of rotation (anticlockwise). B_r leads B_ϕ in phase.

another (marked on the top of Figures 2a and 2b) is rather abrupt, occurring typically between 12 and 15 R_S.

[14] A further difference between the periodic fields in the distended and core regions is that the symmetry of the fields with respect to the equator of the field line is different. In the distended magnetosphere, B_r and B_ϕ have near-equatorial nodes and change sign as they cross the tilted current sheet. The nodes therefore are at the current sheet whose position is defined partly by the orientation of the planet with respect to the solar wind and thus is not precisely at either the planetary equator or the magnetic equator. On the other hand, the perturbations in B_ϕ and B_r in the core region are seen to have more like an antinode in the equatorial region because they are symmetric about the planetary equator. This is illustrated for B_ϕ in Figure 4 in which it is clear that the modulated signals do not change phase across the equator. We show the azimuthal field over a range of magnetic latitude, that is, latitude based on a polar coordinate system centered on a dipole offset 0.037 R_S to the north from the center of the planet. The lack of dependence on latitude was not apparent in the plots of Figure 2 because data shown were from passes that remained within a degree of the planetary equator. However, it is clear from Figure 4 that not only does the amplitude of the perturbations in the core region vary little with radial distance between 2.7 and 12–15 R_S on multiple orbits, it also varies little with latitude over the range ±30° magnetic latitude.

[15] In Figure 5, we display the azimuthal cam field B_ϕ for each periapsis pass through the core region between January and August 2006. The azimuthal component B_ϕ is plotted against a phase angle in radians, each periapsis pass (R < 15 R_S) lasting just less than five cycles. The phase in question has been constructed using a formula for describing the Saturn Kilometric Radiation (SKR) periodicity that was put forward by Lecacheux and coworkers and then further developed within the Cassini radio and plasma wave team [*Kurth et al.*, 2007]. The basic period assumed by Kurth et al. is 0.4497 d or 10 h 47 min 34 s). Writing the time-dependent correction to the phase (in radians) as $\Phi_{SKR}(t)$, one has [*Kurth et al.*, 2007]

$$\Phi_{SKR}(t) = \left(87.77 - 2.527 \times T_d + 3.041 \times 10^{-3} \times T_d^2 - 7.913 \times 10^{-7} T_d^3\right) \times (\pi/180) \quad (1)$$

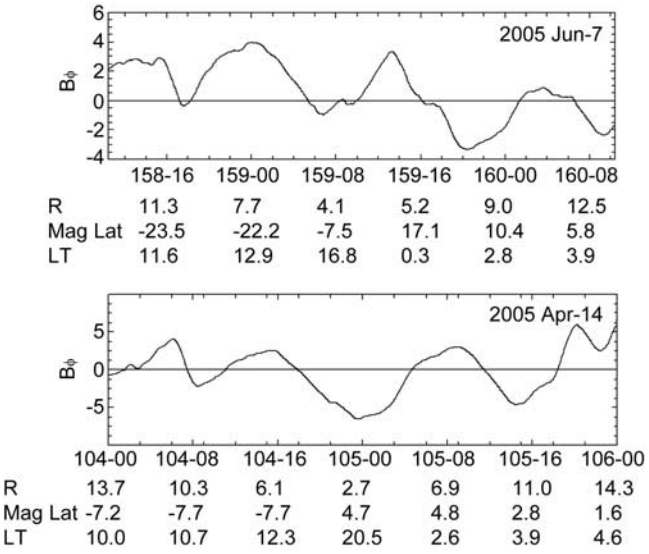

Figure 4. Illustration of the lack of variation in the cam signal with both radial distance and latitude. The plots come from passes in June and April 2005, respectively, and both are for radial distances R < 13 R_S. Shown is (top) the magnetic latitude (measured with respect to the spin axis and a point 0.037 R_S north of the planetary center, consistent with the standard SPV field model) ranges between ±20°. (bottom) The latitude range in the lower pass is smaller but the closest approach is much closer at 2.7 compared with 3.6 R_S. The panels below the plots indicate radial distance, magnetic latitude, and local time (range 0–24 h).

where T_d is the time in days measured from 1 January 2004. *Kurth et al.* [2007] propose a system of planetary longitude based on the phase. The constant term in the expression, 87.7 (in degrees), was chosen to make the longitude formula consistent with the original radio-based longitude system [*Desch and Kaiser*, 1981] wherein the peak of the SKR signal is detected when longitude 100° is the subsolar longitude (using the conventional west longitude).

[16] We do not concern ourselves with a longitude system here but rather the nature of the phase variation. *Kurth et al.* [2007] describe the SKR signal as not rotating with the planet [*Warwick et al.*, 1981; *Gurnett et al.*, 1981], but it is most unlikely that the magnetic cam signal is pulsing in the way that the SKR is. The deductions of *Espinosa et al.* [2003b] and *Cowley et al.* [2006] make sense only if the signal represents a rotating structure. Accordingly, the phase $\Phi_M(t)$ used in Figure 5 and subsequent figures has been adjusted for the spacecraft position as if the planet/SKR source is rotating underneath. Hence $\Phi_M(t)$ is given in radians by:

$$\Phi_M(t) = 13.97\ T_d - \Phi_{SKR}(t)\left(\frac{LT-12}{12}\right) \times \pi \qquad (2)$$

and multiples of 2π can be omitted. In Figure 5 it is clear that $\Phi_M(t)$, including a correction for the local time of observation, does a good job of organizing the data and it shows that the assumption that the magnetic signal has a strong rotational element is correct. It is, however, not perfect. The continuous red trace, a cosine guide signal of amplitude 2 nT closely phased to the magnetic B_ϕ signal, shows the limitations. The guide signal is based on the sinusoidal match to the B_ϕ signal that will be discussed later (see Figure 7). The continuous curve aligns with the lowest latitude peak of B_ϕ and its peak passes through midday with a phase delay of order 60° (with respect to the time of the SKR pulse). The actual signal is not a perfect sinusoid and there are small phase shifts between it and the guide signal. Some shifts appear systematic and are to be studied in a subsequent paper. Other phase shifts appear to be random (jitter). The dashed curve is a second sinusoid that follows the point in planetary "longitude" thought to correspond to the SKR peak [see *Kurth et al.*, 2007]. What this means is that the signal varies with the predicted radio frequency and it peaks when a specified "longitude" passes through the subsolar meridian (1200 LT). As the SKR appears to pulse rather than rotate, caution is needed in interpreting what, if anything, is rotating.

[17] In Figure 6 we show data from the same period in which the cam radial component (middle) is shown for comparison with the azimuthal component (top). The vertical lines illustrating the SKR phase in a rotating frame in Figure 6 have been shifted to align with the rotating peak in B_ϕ. The background offset dipole field (SPV model) has been subtracted from the radial component. The radial component is also affected by what appears to be an (azimuthally) uniform ring current, the effect of which is to produce a small latitude dependence in the nonoscillatory (background) field. Empirically, the effect of the ring current has been removed by subtracting a field

$$\Delta B_r(\lambda_m) = -0.2 \times \lambda_m(\mathrm{nT}) \qquad (3)$$

where λ_m is the magnetic latitude (measured in degrees positive northward from an equatorial origin offset along the planetary spin axis by 0.037 R_S as in the SPV model field [*Davis and Smith*, 1990]). This is a purely empirical choice made to remove from the signal the first-order variation in ΔB_r with respect to latitude.

[18] The lower panel shows superposed plots of the spacecraft radial distance and local time. The radial penetration is similar from orbit to orbit with periapsis near 5 R_S. The surprising fact revealed by the plot is that the periapses have a tendency to be within a quarter cycle of an even multiple of π (i.e., near an antinode of the cosine). This is a chance artifact of the orbital periods. It has an effect in the data. Figure 7 shows that B_ϕ has a peak in phase with the cosine guide signal and so the data tend to show a peak in that component near closest approach. Correspondingly, there is a node in the radial component regularly near periapsis. Nonetheless, the amplitude of the B_r cam signal does seem to decrease near closest approach, a point that will be studied later with a wider range of passes. The similarity of the LT plots also indicates that the line of apsides does not move far around the planet from orbit to orbit during the 8 month period here analyzed. The plots reveal clearly the fairly systematic phase relationship (B_r leads B_ϕ by a quarter cycle). The spread in the overlaid

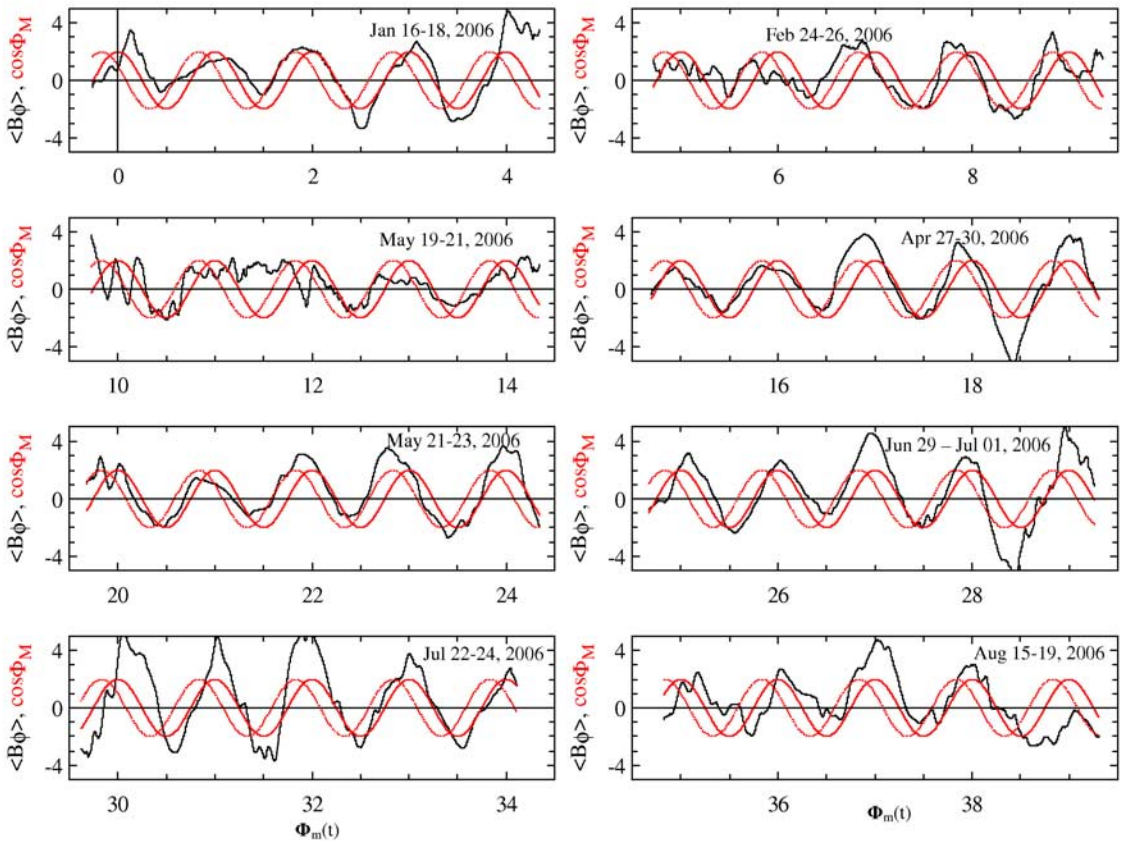

Figure 5. Azimuthal component B_ϕ recorded for each periapsis pass between January and August 2006 plotted against $\Phi_M(t)$, the LT-adjusted (see text) phase of the SKR periodicity of the epoch. The dashed red traces represent a notional signal rotating at the model frequency (as described in the text) of the predicted SKR radio signal pulse. Derived from long-term averaged data, the actual SKR pulse is predicted to occur as the peak of the signal shown passes through midday. The continuous line is a signal of the same frequency shifted in phase by 60° to match more closely the phase of the rotating peak in B_ϕ. The data are taken from 15 R_S radial distance inbound through closest approach just inside 5.5 R_S and out to 12.5 R_S radial distance outbound. The spacecraft remains within 5° of the equator throughout.

signals also reveal that the jitter in the signal is as much as a quarter cycle.

[19] Figure 7 plots the same data in yet a different way. Here the B_ϕ data from the January to August periapsis passes are plotted against phase within one cycle. The heavy trace once again represents a cosine signal. Here the comparison of the trace with 36 cycles of overlaid data makes a convincing argument for an underlying sinusoidal signal. This plot indicates that, to a good first approximation, the B_ϕ signal varies with planetary longitude as cos ϕ, where ϕ is based on SKR [*Kurth et al.*, 2007] and shifted in phase by 60° as previously described to track the peak in B_ϕ. This has important implications as we shall see in later sections. Accordingly, the cos ϕ variation of B_ϕ would mean that the peak in B_ϕ is approaching the dusk meridian as the SKR peak longitude passes through midday. Recalling that B_r signal peak leads B_ϕ by a quarter cycle, it follows that the SKR peak emission occurs when the peak negative perturbation in B_r is approaching midday. As the SKR source is believed to be localized near midday [*Kaiser and Desch*, 1982], it seems that any link with the magnetic cam signal is likely to be associated with a periodic B_r field perturbation that, at its peak, tilts the field in the midday sector away from the Sun.

4. Cam Field Configuration, Motion, and Displacement

[20] In the following sections we examine the implications of the experimental features of the cam signal elucidated in the previous sections.

[21] We treat first the N–S symmetric nature of the magnetic cam field revealed, for example, by the absence of latitude dependence in Figure 4. Working in an inertial frame, writing the time variation as exp($-i\omega t$) where ω is the angular frequency (2π/period) and using the magnetohydrodynamic (MHD) approximation, the plasma velocity and the field perturbation associated with the dynamic disturbance that the cam represents are linked by the formula

$$-i\omega \mathbf{b} = \nabla \times (\mathbf{u} \times \mathbf{B}) \tag{4}$$

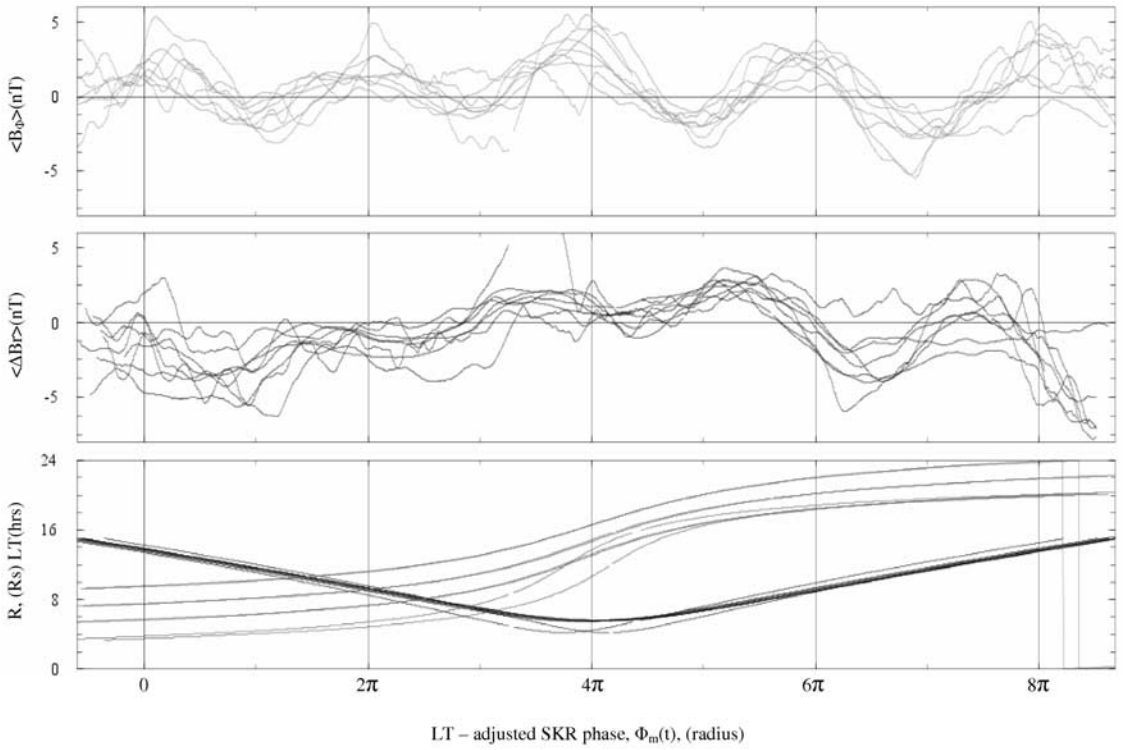

Figure 6. (top) Superposed azimuthal components B_ϕ from the eight passes shown in Figure 5 and (bottom) superposed radial components of the cam disturbance ΔB_r (from which the axisymmetric SPV model field has been subtracted). This component has also been adjusted for the presence of a steady ring current, which introduces an antisymmetric variation with latitude (described in the text). The abscissa in each plot is the SKR phase based on the cubic model of the Meudon and Iowa groups, which has been adjusted for the local time of the spacecraft to account for rotation. The data are taken from within 10 R_S radial distance. Figure 6 (bottom) shows superposed plots of radial distance and LT for each pass. Note that there appears to be a (chance) synchronicity between the Cassini orbital period and the radio period.

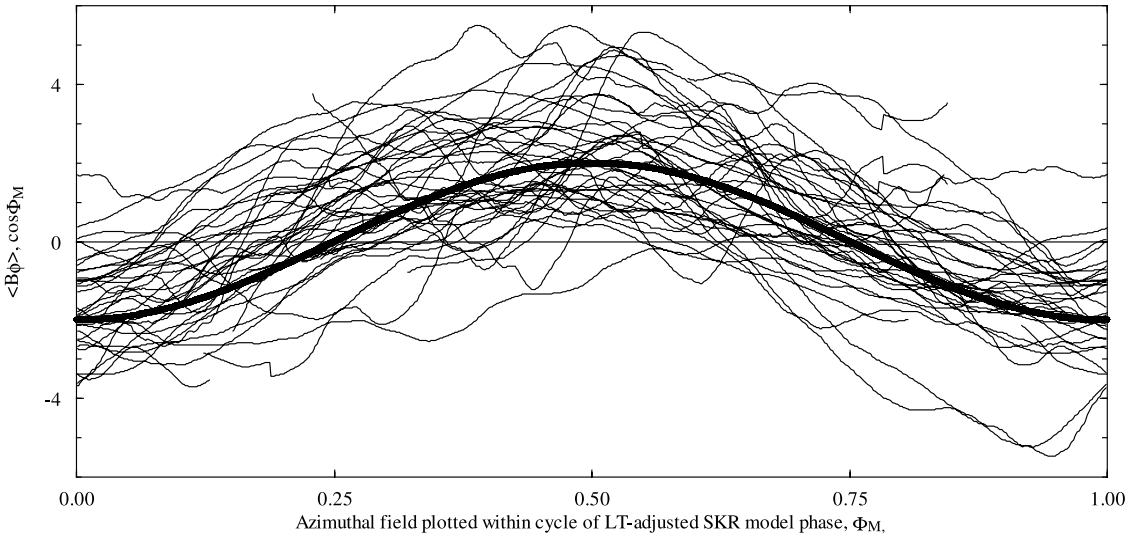

Figure 7. Superposed azimuthal components Bϕ from the eight passes shown in Figure 5 plotted against SKR phase adjusted for spacecraft local time to account for rotation (as described in the text) and then reduced to one cycle. The data are taken from within 15 R_S radial distance. Also shown (heavy trace) is a plot of the cosine of the phase.

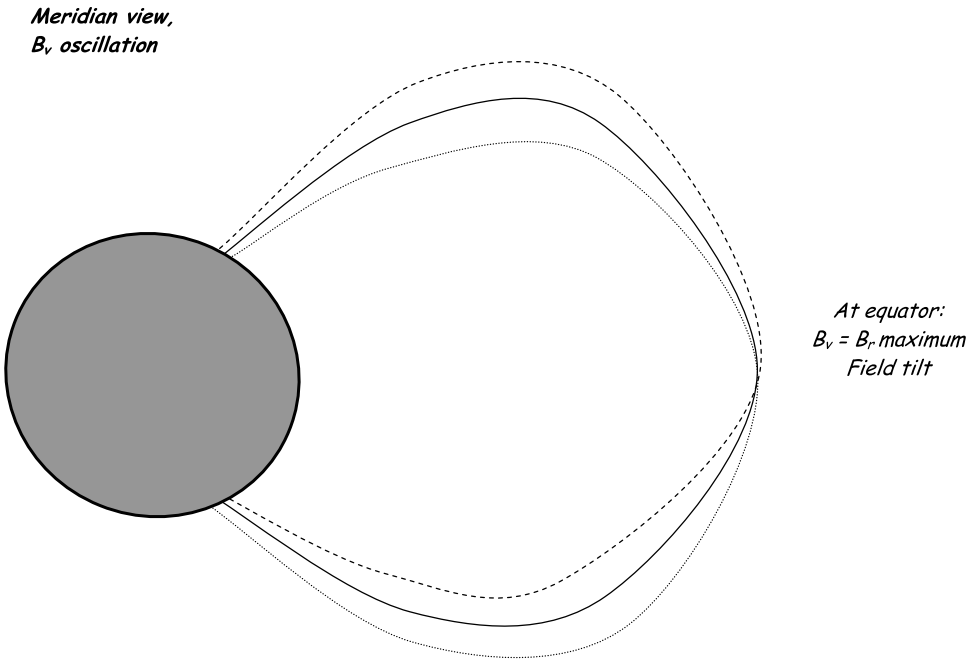

Figure 8a. Illustration of the extrema (dotted line and dashed line) of field line displacements in the meridian plane. As the magnetic signal is symmetric about the equator, the displacement is asymmetric and the field line displacement has a node there.

[22] It is useful to introduce the plasma displacement, $\boldsymbol{\xi}$, where

$$\mathbf{u} = -i\omega\boldsymbol{\xi}$$

which leads to a direct relation between the field perturbation and the displacement

$$\mathbf{b} = \nabla \times (\boldsymbol{\xi} \times \mathbf{B}) \tag{5}$$

[23] Introducing a coordinate, s representing distance along the background dipole field, and coordinates transverse to the field in the azimuthal direction (ϕ) and in the meridian (ν) one can extract expressions for the radial and azimuthal components [see, e.g., *Singer et al.*, 1981]

$$b_\nu = \frac{1}{rB\sin\phi}\mathbf{B}.\nabla(\xi_\nu rB\sin\phi) = \frac{1}{r\sin\phi}\frac{\partial}{\partial s}(\xi_\nu rB\sin\phi) \tag{6a}$$

$$b_\phi = r\sin\phi\mathbf{B}.\nabla\left(\frac{\xi_\phi}{r\sin\phi}\right) = rB\sin\phi\frac{\partial}{\partial s}\left(\frac{\xi_\phi}{r\sin\phi}\right) \tag{6b}$$

where s is distance measured along the background dipole field, conventionally measured from the equator. As might be expected, the azimuthal field and displacement are directly linked and similarly for the meridional component (which will be close to the radial direction wherever the main field is in the B_θ direction). The presence of the parallel differential coefficient, $\partial/\partial s$, in both equations means that the symmetry of the field perturbation about the equator is opposite to the symmetry of the displacement. In Figures 8a and 8b, the sketch shows the consequence of opposite symmetry implied by equations (6a) and (6b). The field displacement is drawn antisymmetric and the field perturbation symmetric with respect to the equator ($s = 0$). The symmetry of the magnetic perturbation is implied by

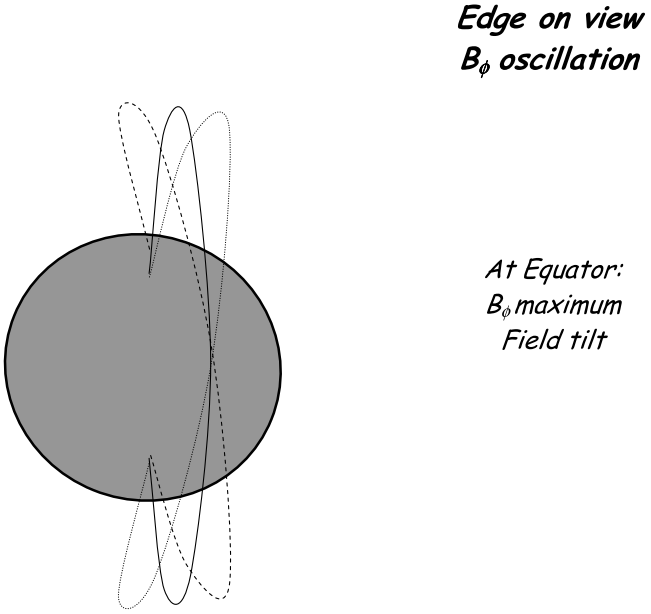

Figure 8b. Illustration of the extrema of field line displacements (dotted line and dashed line) in the azimuthal direction. As in Figure 8a, because the azimuthal field component is symmetric about the equator, the displacement is asymmetric. As in the meridian motion, again the field line displacement has a node at the equator.

the lack of dependence on latitude. It follows that the displacement is antisymmetric.

[24] The sketches show extrema of field line displacement in the meridian plane. (Figure 8a illustrates perturbations in B_r) and in the azimuthal direction (Figure 8b illustrates perturbations in B_ϕ.) In addition, one can bear in mind that, as the hodogram in Figure 3 shows, the overall motion near the equator is a coning of the field about the mean field direction. The equatorial point (where by symmetry there is no displacement) being the apex. Figure 3 shows directly that B_ϕ leads B_r. One can note that the same will apply to the displacement and the velocity; the sense of rotation is anticlockwise (right-handed) looking along the field.

[25] As the symmetry and the figures make clear, the displacement (and the velocity) at the end of the flux tube in the northern hemisphere associated with the signal is opposite to that in the southern hemisphere. What sort of global plasma motion is implied by this and what could excite it?

[26] In fact, the observations are most easily understood if there is a steady background motion, in addition to corotation, that perturbs the field very little. Such motions are familiarly known as interchange motions, which in the ideal limit do not produce changes of the field. They can occur wherever the background field pressure is much larger than the plasma pressure so that redistribution of plasma does not change the field. For such motions the left-hand sides of (6a) and (6b) vanish and

$$\frac{1}{r\sin\phi}\frac{\partial}{\partial s}(\xi_r rB\sin\phi) = rB\sin\phi\frac{\partial}{\partial s}\left(\frac{\xi_\phi}{r\sin\phi}\right) = 0 \qquad (7)$$

Such displacements can arise spontaneously (through the interchange instability) where there is a plasma source deep inside the magnetosphere [see, e.g., *Southwood and Kivelson*, 1987, 1988]. *Gurnett et al.* [2007] have found persuasive evidence that there is a longitudinal asymmetry in the plasma distribution in the inner magnetosphere, in the vicinity of the E-ring and the orbit of the moon Enceladus, that rotates in concert with both the radio and magnetic cam signals. They propose that there is a rotating two cell circulation (outward transport in one longitude sector and inward in the other) based on spontaneous interchange motion maintained by the continual process of ionization of material ejected from rings and moon.

[27] *Goldreich and Farmer* [2007] have independently put forward a similar theoretical idea to that proposed by *Gurnett et al.* [2007] to explain their observations. Their proposal invokes a rotating two cell circulation pattern of flux tubes (like Gurnett et al.). However, their view that such a pattern could explain the cam magnetometer signal is ill-founded. The field displacement and therefore plasma velocity has to be either outward or inward at all points on a flux tube anywhere in the circulation. However, as we showed above, the N–S symmetry of the cam field perturbation implies a N–S asymmetry of the displacement (and hence plasma velocity). In other words, at times when the perturbation velocity associated with the cam magnetic signal in the northern hemisphere is outward, it must be inward in the southern hemisphere and vice versa. In the context of a global two-cell rotating convection system, the cam signal would at best be a secondary effect due to a north–south asymmetry in the ionospheric conductivity or drag exerted on the motion of the interchanging flux tubes. This interpretation is discussed later.

5. Source of a Quasi-Uniform Magnetic Cam Field

[28] We next examine the implications of the cos ϕ dependence of the cam signal that was deduced from Figure 7. The sinusoidal variation carries with it some important message regarding symmetry. Not only does it indicate that the ultimate source is in some way associated with the planet and its rings (which share a common axial symmetry) rather than a source external to the system but also the absence of higher-order harmonics indicates that the source is relatively simple.

[29] The relatively uniform nature of the cam adds to this conclusion. Just as the dipole is the simplest internal source for a system with spherically symmetric boundary conditions, so a uniform field is the simplest external field. In vacuum, both are derived from a potential (V) varying as cos ϕ where ϕ is azimuth, namely,

$$V = \frac{A\cos\phi}{r^2}\ \text{(dipole)},\ Cr\cos\phi\ \text{(constant field)} \qquad (8)$$

A magnetosphere is not a vacuum but nonetheless, the currents that determine the field usually flow in fairly limited volumes of space. Currents flow in sheets (e.g., the cross-tail current sheet, the magnetopause boundary currents) or in localized spatial regions (the auroral or cusp field-aligned currents). In a rotating magnetosphere even the ring current tends to be confined to the equatorial regions by the centrifugal effects.

[30] The second form in equation (4) represents a constant field; if such a field rotates with the planet, it produces sinusoidally varying radial and azimuthal signals of equal amplitude, approximately what is observed in the core region of the magnetosphere. The discovery that the cam shaft signal is quite sinusoidal as shown in Figure 7 and changes little with latitude or radial distance as shown in Figure 4 fits very directly with the uniformity of the field in latitude (at least up to ±30°).

[31] The low-order variation about the planetary axis is required by the observations. Higher-order terms for an external source would vary more strongly with R (as R^n with $n \geq 2$) and, even if weak near the planet, would grow with distance and undermine not only the cos ϕ dependence of the signal but also its relative uniformity with R.

6. Deductions Concerning Forces, Momentum Transfer, and Currents

[32] The presence throughout a large region of space of the quasi-constant cam magnetic field has implications for the stress in that volume. In a magnetosphere, magnetic forces are inevitably important and one may picture the forces and momentum being transmitted by using the Maxwell magnetic stress tensor. Again taking a coordinate system based on the background dipole field, $\mathbf{B_d}$, we can see that wherever the B_ϕ field is present there is an off-diagonal component of the stress tensor, $B_\phi B_d$. The presence

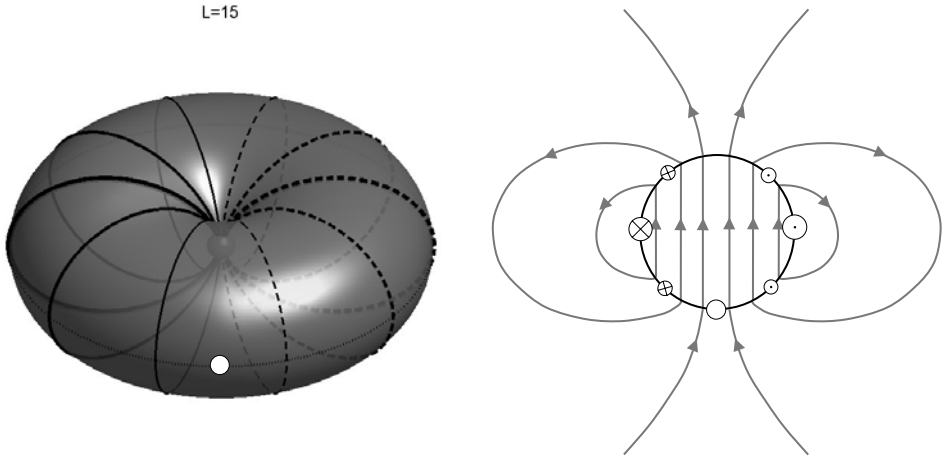

Figure 9. (left) Schematic shell of dipolar field lines at L ~15 R_S on which currents flow into and out of the northern ionosphere. If the current strength varied sinusoidally with longitude, as indicated by varying thickness of the lines representing the current, but flowed on a spherical surface, the perturbation field within the shell would be uniform. In order to produce the observed uniform field within a nonspherical surface, additional current loops must be present on the surface. (right) In a cut through the equatorial plane, field lines arising from the field-aligned currents at L = 15 shown in the left hand diagram. The field is uniform in the shaded area inside the shell at L = 15 (here shown on a different scale) and dipolar outside of that boundary. The white dots in the two images are at the same location on the boundary.

of the component means that there is a flux of azimuthal momentum along the background field direction. The sense of transport reverses as B_ϕ reverses in each cycle. Since the background field points southward at the equator, momentum in the direction of the planetary rotation is being transported from the northern to the southern hemisphere whenever B_ϕ is positive. One can make a similar set of arguments concerning the transport along the background field of momentum in the meridian by the oscillating meridional component represented by ΔB_r.

[33] Wherever the stress has a spatial gradient, electric current is flowing. Where currents flow across the field, momentum is being deposited and forces are acting. On the magnetic shells at the outer edge of the cam with equatorial crossing points at 12–15 R_S radial distance, there must be field gradients. However, here the currents associated with a gradient in the meridian of B_ϕ, $\partial B_\phi/\partial \nu$, flow along the field direction and so there are no forces. Accordingly, one envisages the B_ϕ as well as the ΔB_r of the rotating cam field being "switched off" at the outer edge by sheets of field-aligned current. As overall normal field continuity must be maintained across the shell containing the current, beyond the sheet a dipole field will appear which will rotate in the same manner as the cam.

[34] If there is current flow from ionosphere to ionosphere, closure is expected to be through transverse currents in the ionospheres. The forces associated with such currents represent sources and sinks of the momentum transfer along the field inherent in the presence of the cam signal as described above.

[35] The conductivity of a plasma is very high along the field and, although one cannot prove it here absolutely, it is most likely that such a current system would be guided by the field from ionosphere to ionosphere and that the outer boundary of the cam region would correspond to a magnetic shell. Hence the pattern of source current that is consistent with all features so far reported is a system of rotating field aligned currents on magnetic shells with $L \sim 12$–15. Figure 9 shows schematically a magnetic shell for a dipolar form of the magnetic background magnetic field on which the main cam source currents flow, enclosing the cam field. The field-aligned currents that would have to flow from ionosphere to maintain a quasi-constant field inside the shell are sketched also. Additional current loops needed to maintain continuity of the normal component of the field would flow on the surface, but they are not shown.

[36] The fact that the currents associated with the cam field seem to have to flow from ionosphere to ionosphere greatly adds to the difficulty of identifying a plausible mechanism for their generation. Why should a current system of the form sketched in Figure 9 develop? It is most common to think of field-aligned current flow transferring stress from the ionosphere to equatorial magnetosphere to maintain the magnetosphere in rotation with the planet. However, in this case, the primary angular momentum transfer must be between northern and southern hemispheres. In an ionosphere, rotation is imposed through the collisional interaction between ionospheric plasma and the underlying atmosphere; the rotating reference frame is that of the underlying atmosphere whose inertia is assumed to be sufficiently great that it can usually supply whatever mo-

mentum is needed to spin up the plasma. Within the ionosphere, regions of high conductivity are tightly coupled to the atmosphere, but regions of lower conductivity may lag atmospheric rotation. It follows that if the ionospheric conductance differs between the two hemispheres, field-aligned current flow is set up between the ionospheres in order to maintain the same angular velocity on the entire flux tube. Anything that led to different conductance in the northern and southern ionospheres could therefore require field-aligned currents linking them, but we require not only that the currents flow but also that there be a longitude-dependence of the current system. If there were a global asymmetry in which the ionospheric conductance varied sinusoidally with longitude in one ionosphere, the current system could take the qualitative form shown in Figure 9. This seems unlikely unless the asymmetry is controlled by something that is rooted in the planet, a possible candidate being the magnetic field. Arguing against this interpretation is the rate of drift of the period of the signal, which seems too rapid to be associated with such an internal source.

7. At Large Distances: An Effective Tilted Dipole

[37] As we describe above, a quasi-uniform field on the shells of the quasi-dipolar region of the magnetosphere generates a rocking field where the rocking increases as a function of distance from the planet. The angular tilt, α at the equator in the meridian is given by

$$\alpha = \arctan\left(\frac{\Delta B_r}{B}\right) = \arctan\left(\frac{L^3 \Delta B_r}{B_0}\right) \approx \frac{L^3 \Delta B_r}{B_0}$$

where B_0 is the equatorial field at the planetary surface (of order 20,000 nT) and L is the equatorial radial distance in units of R_S. It follows that as long $\|\Delta B_r\| \ll B_o / L^3$, the tilt increases proportional to L^3. As the cam signal strength is of order 2–3 nT and the field remains approximately dipolar inside of $L \approx 12$–15, one concludes that the condition is always satisfied in the core region and moreover that the tilt induced at the outer edge of the signal is of order 2–3/10 [$\sim 13^3/(2 \times 10^4)$] or as much as 12°–18°. Beyond the shells where the field-aligned currents flow, the cam is replaced by a rotating signal which has a dipole signature. In this region the planet would appear to have a dipolar field with a tilt (with respect to the rotation axis) that would be fixed at the maximum value achieved.

8. Comments on the Distant Magnetosphere

[38] As we noted in the last section, the current system associated with the cam signal consists of a shell of field-aligned current flowing on L-shells near 12–15 with a sinusoidal variation with longitude, while on shells crossing the equatorial plane beyond $\sim$12–15 R_S the signature of the current system should resemble that of a rotating equatorial dipole moment (see Figure 9). It follows from the estimate in the previous paragraph that at large distances (>12–15 R_S), the net dipolar perturbation of the Saturnian field should appear to rock by more than 12°.

[39] Hence we have a mechanism providing an equivalent to a rocking dipole on high latitude flux tubes. In the distant magnetosphere, the region where the equatorial current sheet dominates, many features of the temporal variations will appear similar to those familiar at Jupiter where there is an actual tilted (and offset) planetary dipole. In particular, the tilt of the total field (arising from internal and external sources) results in periodic displacement of the center of the current sheet in the distended magnetosphere. The different phase relations between B_r and B_ϕ recorded beyond 12–15 R_S in the distended tail-like configuration are easily understood in the context of the comparison to Jupiter. There is a central plasma disk that moves up and down relative to the spacecraft [*Hill et al.*, 1981; *Vasyliunas*, 1983]. Others have reported similar flapping of the distant current sheet at Saturn and have attributed the flapping to a tilted internal field (K. K. Khurana and C. Arridge, personal communication, 2006).

[40] However, a feature that may be different is the overall transport. There are known to be significant sources of neutral and ionized material from the rings and the plume of Enceladus [*Dougherty et al.*, 2006; *Jones et al.*, 2006; *Tokar et al.*, 2006], which might be seen as analogous to the Io torus at Jupiter. There are likely to be limits to the analogy. The discovery of a plasma asymmetry close to the planet by *Gurnett et al.* [2007] in the region of the plasma source indicates that the dominant transport of plasma in the core magnetosphere is through a rotating two-cell circulation system driven by interchange instability. Moreover, one expects that the two-cell imposition of a outward moving sector and an inward moving sector of depleted tubes where magnetic flux returns might be imposed throughout the magnetosphere including the distended field region. There is indeed some evidence of a planetary longitude dependent circulation in the distended field region, a topic that will be addressed in a subsequent paper.

9. Sources of Interhemispheric and Longitudinal Variation of Ionospheric Conductance

[41] We have already mentioned some potential explanations of the results presented here. Our observations seem to require that in one hemisphere the ionospheric conductance varies with longitude and that there are differences in conductance between the two hemispheres in regions linking magnetically to the equator inside of 15 R_S. Conductivity depends inversely on the strength of the magnetic field, on the plasma density, and on properties of the underlying atmosphere. Accordingly, non-uniform conductivity could result from variation of any of these properties with longitude. We find it difficult to argue that the ionospheric plasma density can have a strong and relatively stable variation with longitude. It is easier to imagine that an internal magnetic multipole could produce longitudinal variations of conductivity. However, a field extremum in some range of longitude is not consistent with analysis of data taken close to the planet [*Connerney et al.*, 1982; *Giampieri et al.*, 2006], although a multipole of order octupole or higher could have escaped detection. However, a high-order multipole is difficult to fit with the cos ϕ azimuthal dependence of the signal because it is not clear how a high-order magnetic anomaly could give rise to the low-order sinusoidal nature of the cam signal. Moreover, we again note that one does not expect internal magnetic structures to drift sufficiently rapidly to account for the

observed variation of the period over a timescale of years [*Gurnett et al.*, 2005; *Kurth et al.*, 2007].

[42] If the source is not internal to Saturn, it is possible that the longitudinal variation is linked to properties of the underlying atmosphere. In this case, the observed period would not reflect the interior rotation rate but the rate of rotation of the ionosphere and the atmosphere to which it is coupled. The atmospheric wind speed is known to have changed over timescales of years. *Sanchez-Lavega et al.* [2003] report that the long-term behavior of the winds at Saturn is stable in time to about 10%, but they report that the speed of the equatorial jet dropped by about 200 m/s from 1996 to 2002. Other measured jets in the southern hemisphere remained stable relative to the observations made by Voyager in 1980–1981 but there is little data on the jets at high northern latitudes. However, there are difficulties with any such argument as a simple jet might be expected to polarize in such a way that a reverse sheet of field-aligned current would form at the low-latitude edge of the jet such that only the shells threading the jet would be accelerated. More work is required to elucidate this possibility.

[43] Despite some possible clues, there remains at the moment no clear theory to explain the steady evolution in the magnetic period as originally indicated in the SKR signal and, correspondingly, no theory relying on the structure of internal current sources to account for the cam signal and its changing periodicity.

[44] In interpreting the field aligned currents flowing on external magnetic shells, we have also alluded to differences in ionospheric conductance in the two hemispheres, recognizing that the drag exerted on magnetospheric plasma is proportional to the ionospheric conductance. Because ionospheric conductivity is photo-sensitive, N–S asymmetry could arise from differing lighting conditions. The ionosphere in either hemisphere suffers a seasonal change in illumination from the tilt of the rotation axis and also from the shadowing effect of the rings. At present Saturn's magnetic (and rotation) axis is in a northern winter configuration, with the north pole tilted away from the Sun. The dayside northern hemisphere at high latitude is in darkness because of the tilt and the rings cast a shadow at lower latitudes in the northern hemisphere, so an interhemispheric asymmetry of conductance is plausible. However, periodic perturbations of the magnetic field in the core magnetosphere were also observed during the Pioneer 11 and Voyager 1 and 2 passes. Although the illumination of the northern and southern hemispheres was also asymmetric during those passes, the differences were far less extreme than during the Cassini tour because Saturn's spin axis orientation was relatively close to equinoctial. This calls into question an interpretation based on asymmetries imposed by ionospheric illumination.

[45] The north–south asymmetry of the cam and its relation to the SKR signal remains puzzling in other respects. If the SKR signal emerges from solar wind-Saturn interaction, as is generally assumed, at the present epoch it seems to occur when the phase of peak radial field is approximately oriented away from the Sun. This would correspond to the tilt direction that would most decrease the internal magnetospheric field pressure near the magnetopause in the hemisphere facing the Sun. How this change can affect the SKR signal is a matter that will be further elucidated elsewhere.

10. Conclusions

[46] The paper has examined the periodically varying component of the magnetic field seen in the near equatorial magnetosphere inside of $\sim$15 R_S during each Cassini spacecraft periapsis pass for the first 24 orbits of the mission. The field perturbation has been found to be remarkably uniform both with respect to radial distance and latitude, at least up to 30° off the equator. The phase relations between the transverse magnetic field components make it clear that the signal is generated by a source external to the planet. The current system described here is the minimum required to account for the presence of the cam magnetic field in the core magnetosphere. It also explains the features of the distended magnetosphere, where the same currents mimic a rocking planetary dipole. The same field-aligned currents are also likely to be the source of the Saturn kilometric radio signals that are modulated in a similar manner to the magnetic field. At this point no description of the origin of the currents themselves seems yet fully satisfactory.

[47] The recent discovery of a longitudinal asymmetry in the plasma deep within the magnetosphere [*Gurnett et al.*, 2007] is also certainly linked. However, the relationship between the cam signal, whose driving currents flow from ionosphere to ionosphere, and a two-cell circulation driven from plasma gradients in the magnetosphere also remains to be further elucidated.

[48] **Acknowledgments.** We are grateful to Michele Dougherty for encouraging us to complete this paper and for providing invaluable data on which it is based. Discussions with K. K. Khurana and V. M. Vasyliunas were most helpful to the authors. We are grateful to X.-Z. Jia for creating Figure 9. This work was partially supported by the Division of Atmospheric Sciences of the National Science Foundation under grant ATM-02-05958. UCLA Institute of Geophysics and Planetary Physics publication 6338.

[50] Wolfgang Baumjohann thanks Stanley Cowley and Vytenis M. Vasyliunas for their assistance in evaluating this paper.

References

Acuna, M. H., and N. F. Ness (1980), The magnetic field of Saturn–Pioneer 11 observations, *Science*, *207*, 444–446.

Acuna, M. H., J. E. P. Connerney, and N. F. Ness (1981), Topology of Saturn's main magnetic field, *Nature*, *292*, 721–724.

Cecconi, B., and P. Zarka (2005), Model of a variable radio period for Saturn, *J. Geophys. Res.*, *110*, A12203, doi:10.1029/2005JA011085.

Connerney, J. E. P., N. F. Ness, and M. H. Acuna (1982), Zonal harmonic model of Saturn's magnetic field from Voyager 1 and 2 observations, *Nature*, *298*, 44–46.

Cowley, S. W. H., D. M. Wright, E. J. Bunce, A. C. Carter, M. K. Dougherty, G. Giampieri, J. D. Nichols, and T. R. Robinson (2006), Cassini observations of planetary-period magnetic field oscillations in Saturn's magnetosphere: Doppler shifts and phase motion, *Geophys. Res. Lett.*, *33*, L07104, doi:10.1029/2005GL025522.

Desch, M. D., and M. L. Kaiser (1981), Voyager measurement of the rotation period of Saturn's magnetic field., *Geophys. Res. Lett.*, *8*, 253–256.

Davis, L., Jr., and E. J. Smith (1990), A model of Saturn's magnetic field based on all available data, *J. Geophys. Res.*, *95*, 15,257–15,261.

Dougherty, M. K., et al. (2004), Cassini magnetic field investigation, *Space Sci. Rev.*, *114*, 331–383.

Dougherty, M. K., et al. (2005), Cassini magnetometer observations during Saturn Orbit Insertion, *Science*, *307*, 1266–1270.

Dougherty, M. K., K. K. Khurana, F. M. Neubauer, C. T. Russell, J. Saur, J. S. Leisner, and M. E. Burton (2006), Identification of a dynamic atmosphere at Enceladus with the Cassini Magnetometer, *Science*, *311*, 1406–1409.

Espinosa, S. A., and M. K. Dougherty (2000), Periodic perturbations in Saturn's magnetic field, *Geophys. Res. Lett.*, *27*, 2785–2788.

Espinosa, S. A., D. J. Southwood, and M. K. Dougherty (2003a), Reanalysis of Saturn's magnetospheric field data view of spin-periodic perturbations, *J. Geophys. Res.*, *108*(A2), 1085, doi:10.1029/2001JA005083.

Espinosa, S. A., D. J. Southwood, and M. K. Dougherty (2003b), How can Saturn impose its rotation period in a noncorotating magnetosphere?, *J. Geophys. Res.*, *108*(A2), 1086, doi:10.1029/2001JA005084.

Galopeau, P. H. M., and A. Lecacheux (2000), Variations of Saturn's radio rotation period measured at kilometer wavelengths, *J. Geophys. Res.*, *105*, 13,089–13,102.

Giampieri, G., M. K. Dougherty, E. J. Smith, and C. T. Russell (2006), A regular period for Saturn's magnetic field that may track its internal rotation, *Nature*, *441*, 62–64, doi:10.1038/nature04750.

Goldreich, P., and A. J. Farmer (2007), Spontaneous symmetry breakingof the external field of Saturn, *J. Geophys. Res.*, *112*, A05225, doi:10.1029/2006JA012163.

Gurnett, D. A., W. S. Kurth, and F. L. Scarf (1981), Plasma waves near Saturn: Initial results from Voyager 1, *Science*, *212*, 235–239.

Gurnett, D. A., et al. (2005), Radio and plasma wave observations at Saturn from Cassini's approach and first orbit, *Science*, *307*, 1255–1259.

Gurnett, D., A. A. M. Persoon, W. S. Kurth, J. B. Groene, T. F. Averkamp, M. K. Dougherty, and D. J. Southwood (2007), The rotation of the inner region of Saturn's plasma disk, *Science*, *309*, 442–445, doi:10.1126/science.1138562.

Hill, T. W., A. J. Dessler, and L. J. Maher (1981), Corotating magnetospheric convection, *J. Geophys. Res.*, *86*, 9020–9028.

Jones, G. H., E. Roussos, N. Krupp, C. Paranicas, J. Woch, A. Lagg, D. G. Mitchell, S. M. Krimigis, and M. K. Dougherty (2006), Enceladus's varying imprint on the magnetosphere of Saturn, *Science*, *311*, 1412–1415.

Kaiser, M. L., and M. D. Desch (1982), Saturnian kilometric radiation: Source locations, *J. Geophys. Res.*, *87*, 4555–4559.

Khurana, K. K. (1997), Euler potential models of Jupiter's magnetospheric field, *J. Geophys. Res.*, *102*, 11,295–11,306.

Kurth, W. S., A. Lecacheux, T. F. Averkamp, J. B. Groene, and D. A. Gurnett (2007), A Saturnian longitude system based on a variable kilometric radiation period, *Geophys. Res. Lett.*, *34*, L02201, doi:10.1029/2006GL028336.

Lecacheux, A., P. Galopeau, and M. Aubier (1997), Re-visiting Saturnian radiation with Ulysses/URAP, in *Planetary Radio Emissions IV*, edited by H. O. Rucker, S. J. Bauer, and A. Lecacheux, pp. 313–325, Aust. Acad. of Sci. Press, Vienna.

Mitchell, D. G., et al. (2006), Planetary rotation modulation of various measured plasma parameters in Saturn's magnetosphere: A possible mechanism, *Eos Trans. AGU*, *87*(36), Jt. Assem. Suppl., Abstract P44A-04.

Ness, N. F., et al. (1981), Magnetic field studies by Voyager 1–Preliminary results at Saturn, *Science*, *212*, 211–217.

Paranicas, C., D. G. Mitchell, E. C. Roelof, P. C. Brandt, D. Williams, B. H. Mauk, and S. M. Krimigis (2005), The Compton Getting effect in ENA images of energetic ion injections at Saturn, *Eos Trans. AGU*, *86*(18), Jt. Assem. Suppl., Abstract SM 13A-02.

Sanchez-Lavega, A. S. Perez-Hoyos, J. F. Rojas, R. Hueso, and R. G. French (2003), A strong decrease in Saturn's equatorial jet at cloud level, *Nature*, *423*, 623–625.

Singer, H. J., D. J. Southwood, R. J. Walker, and M. G. Kivelson (1981), Alfven wave resonance in a realistic magnetospheric magnetic field geometry, *J. Geophys. Res.*, *86*, 4589–4596.

Smith, E. J., et al. (1980a), Saturn's magnetic field and magnetosphere, *Science*, *207*, 407–410.

Smith, E. J., et al. (1980b), Saturn's magnetosphere and its interaction with the solar wind, *J. Geophys. Res.*, *85*, 5655–5674.

Southwood, D. J., and M. G. Kivelson (1987), Magnetospheric interchange instability, *J. Geophys. Res.*, *92*, 109–116.

Southwood, D. J., and M. G. Kivelson (1988), Magnetospheric interchange motions, *J. Geophys. Res.*, *94*, 299–308.

Southwood, D. J., A. Balogh, and E. J. Smith (1992), The Dual Technique Magnetometer for the Cassini Orbiter Spacecraft, *J. Brit. Interplanet. Soc.*, *45*, 371–374.

Tokar, R. L., et al. (2006), The interaction of the atmosphere of Enceladus with Saturn's plasma, *Science*, *311*, 1409–1412.

Vasyliunas, V. M. (1983), Plasma distribution and flow, in *Physics of the Jovian Magnetosphere*, edited by A. J. Dessler, pp. 395–453, Cambridge Univ. Press, New York.

Warwick, J. W., et al. (1981), Planetary radio astronomy observations from Voyager 1 near Saturn, *Science*, *212*, 239–243.

M. G. Kivelson and D. J. Southwood, Institute of Geophysics and Planetary Physics, University of California, Los Angeles, 6843 Slichter Hall, 405 Hilgard Avenue, Los Angeles, CA 90095-1567, USA. (mkivelson@igpp.ucla.edu)